nature medicine

Combined treatment with statins and aminobisphosphonates extends longevity in a mouse model of human premature aging

Ignacio Varela[1], Sandrine Pereira[2], Alejandro P Ugalde[1], Claire L Navarro[2], María F Suárez[1], Pierre Cau[2], Juan Cadiñanos[1], Fernando G Osorio[1], Nicolas Foray[3], Juan Cobo[4], Félix de Carlos[4], Nicolas Lévy[2], José M P Freije[1] & Carlos López-Otín[1]

Several human progerias, including Hutchinson-Gilford progeria syndrome (HGPS), are caused by the accumulation at the nuclear envelope of farnesylated forms of truncated prelamin A, a protein that is also altered during normal aging[1,2]. Previous studies in cells from individuals with HGPS have shown that farnesyltransferase inhibitors (FTIs) improve nuclear abnormalities associated with prelamin A accumulation, suggesting that these compounds could represent a therapeutic approach for this devastating progeroid syndrome[3]. We show herein that both prelamin A and its truncated form progerin/LAΔ50 undergo alternative prenylation by geranylgeranyltransferase in the setting of farnesyltransferase inhibition, which could explain the low efficiency of FTIs in ameliorating the phenotypes of progeroid mouse models. We also show that a combination of statins and aminobisphosphonates efficiently inhibits both farnesylation and geranylgeranylation of progerin and prelamin A and markedly improves the aging-like phenotypes of mice deficient in the metalloproteinase Zmpste24, including growth retardation, loss of weight, lipodystrophy, hair loss and bone defects. Likewise, the longevity of these mice is substantially extended. These findings open a new therapeutic approach for human progeroid syndromes associated with nuclear-envelope abnormalities.

The elucidation of some molecular mechanisms underlying human aging has been facilitated by studies on segmental progeroid syndromes such as HGPS[4], a fatal disease for which there is currently no treatment[5]. Most people with HGPS have a single nucleotide substitution within exon 11 of the gene encoding lamin A (*LMNA*)[1], a nuclear protein that undergoes a complex maturation including farnesylation and proteolytic processing by the ZMPSTE24–FACE-1 metalloproteinase[6]. This mutation (GGC→GGT; G608G) activates a cryptic splice-donor site, finally leading to a truncated prelamin A isoform called LAΔ50-progerin[1]. Mutations in *ZMPSTE24* have also been found in some cases of HGPS or related progeroid syndromes that do not have mutations in *LMNA*[1,7]. Notably, *Zmpste24*$^{-/-}$ mice show a premature aging phenotype that phenocopies human HGPS[6,8]. In all cases, the mutations in *LMNA* or *ZMPSTE24* give rise to farnesylated forms of prelamin A that accumulate at the nuclear envelope, leading to the nuclear abnormalities and functional defects of cells from individuals with HGPS and *Zmpste24*$^{-/-}$ mice[1,6,8–11].

Several groups have suggested that FTIs, originally developed as anticancer drugs, could be useful for HGPS therapy[3,12]. Previous studies with HGPS cells have supported this hypothesis[13–18]. Thus, FTIs reduce the incidence of nuclear deformities associated with HGPS[13–16]. Likewise, FTI treatment of *Zmpste24*$^{-/-}$ or *Lmna*$^{HG/+}$ (heterozygous for a targeted HGPS mutation that exclusively yields progerin) mice relieved some premature aging symptoms in these animals[17,18]. However, the benefit of this strategy seems to be limited, as indicated by the fact that prelamin A was almost undetectable with an antibody to lamin A and lamin C (lamin A/C) in cells from treated mice[17,18]. The low *in vivo* efficiency of these FTI-based treatments of progeroid mice may derive from the fact that the FTI concentration in the plasma of treated mice was much lower than that achieved in earlier anticancer studies[17,18]. It is also possible that prelamin A undergoes alternative prenylation by geranylgeranyltransferase I in the setting of farnesyltransferase inhibition, as described previously for oncoproteins such as K-Ras[19], which could help explain the limited benefits observed with FTI-based treatments of *Lmna*$^{HG/+}$ and *Zmpste24*$^{-/-}$ progeroid mice[20]. To evaluate the possibility that effective blockade of prelamin A prenylation requires inhibition of both farnesyltransferase and geranylgeranyltransferase I, we performed western blot analysis of HeLa cells treated with the farnesyltransferase inhibitor FTI-277 the geranylgeranyltransferase I inhibitor GGTI-2147 or both. The simultaneous presence of both inhibitors led to a

[1]Departamento de Bioquímica y Biología Molecular, Facultad de Medicina, Instituto Universitario de Oncología, Universidad de Oviedo, calle Fernando. Bongera s/n, 33006-Oviedo, Spain. [2]Institut National de la Sante et de la Recherche Medicale UMR_S 910, Génétique Médicale et Génomique Fonctionnelle, Université de la Méditerranée, Faculté de Médecine, 13385 Marseille Cedex 05, France. [3]Institut National de la Sante et de la Recherche Medicale U647, ID17, European Synchrotron Research Facility, 6 rue Jules Horowitz, 38043-Grenoble, France. [4]Departamento de Cirugía y Especialidades Médico-Quirúrgicas, and Instituto Asturiano de Odontología, calle Julián Clavería 6, Universidad de Oviedo, 33006-Oviedo, Spain. Correspondence should be addressed to C.L.O. (clo@uniovi.es).

Received 25 February; accepted 15 May; published online 29 June 2008; doi:10.1038/nm1786

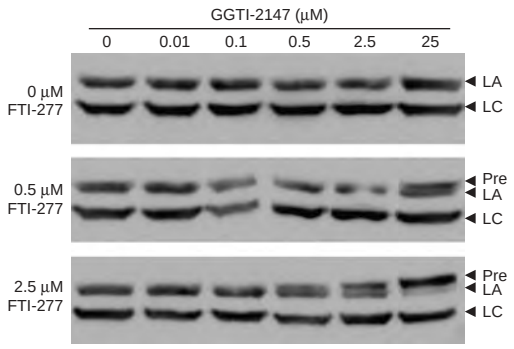

Figure 1 Prelamin A accumulation in the presence of farnesyltransferase and geranylgeranyl transferase inhibitors. Shown is a western blot analysis of lamin A/C in cell lysates prepared from HeLa cells treated with the indicated concentrations of farnesyltransferase inhibitor FTI-277 geranylgeranyltransferase I inhibitor GGTI-2147 or both. LA, lamin A; LC, lamin C; Pre, prelamin A.

substantial accumulation of prelamin A as compared with the effect of each inhibitor alone (**Fig. 1**). To provide direct molecular evidence that prelamin A is alternatively prenylated in the setting of farnesyltransferase inhibition, we performed mass spectrometry analysis of the prenylated prelamin A forms present in *Zmpste24*$^{-/-}$ fibroblasts. We detected the presence of the expected farnesylated and carboxyl-methylated tryptic peptide from prelamin A in *Zmpste24*$^{-/-}$ cells but not in wild-type cells (**Fig. 2a**). This farnesylated peptide lacks the three C-terminal residues Ser-Ile-Met, providing evidence that Zmpste24 is not required for the first proteolytic event occurring during lamin A maturation. Moreover, when we treated cells with FTI-277, we observed a reduction in the amount of the farnesylated peptide from prelamin A (**Fig. 2a**). We next analyzed the section of the spectra corresponding to the putative presence of geranylgeranylated forms of prelamin A peptides. We did not detect any peptide with a molecular mass compatible with this alternative prenylation in prelamin A from untreated *Zmpste24*$^{-/-}$ cells (**Fig. 2b**).

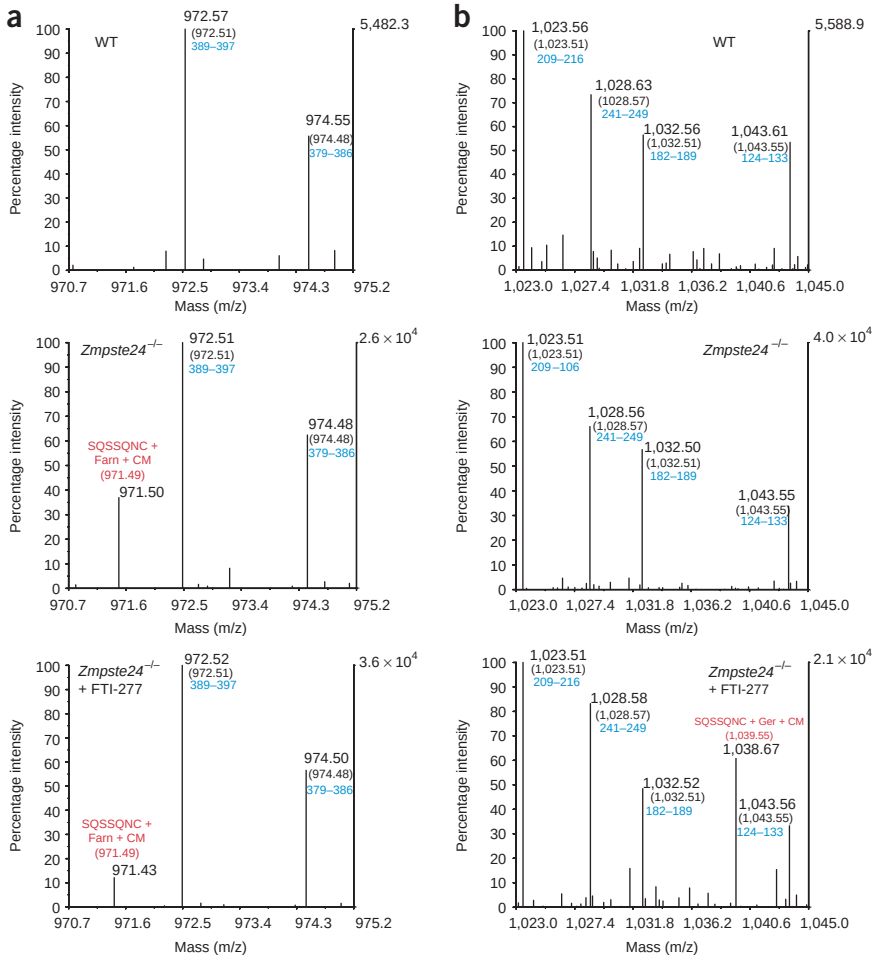

Figure 2 Mass spectrometry analysis of prelamin A alternative geranylgeranylation in the presence of farnesyltransferase inhibitors. We analyzed lamin A (from wild-type cells) and prelamin A (from *Zmpste24*$^{-/-}$ cells) by MALDI-TOF mass spectrometry. (**a**,**b**) Portions of the spectra corresponding to the expected farnesylated (**a**) and geranylgeranylated (**b**) tryptic peptides. Each peak is labeled with the experimental monoisotopic mass, as well as with the theoretical mass (shown in parentheses) of the lamin A or prelamin A tryptic peptides. The residue numbers of the identified peptides are indicated in blue. The amino acid sequence of the prenylated tryptic peptides and their calculated masses are indicated in red. Farn, farnesylated; CM, carboxyl methylated; Ger, geranylgeranylated.

However, after FTI-277 treatment, we detected a peptide whose molecular mass is compatible with the occurrence of a geranylgeranylation event (**Fig. 2b**). To examine whether progerin could also undergo this alternative prenylation in the presence of FTI-277, we extended our analysis to HGPS cells; we found the expected farnesylated and carboxyl-methylated peptide from progerin in these cells but not in wild-type fibroblasts (**Supplementary Fig. 1a** online). Furthermore, treatment of HGPS cells with FTI-277 caused a reduction in the abundance of the farnesylated peptide and the appearance of a new peptide whose molecular mass corresponds to the geranylgeranylated and phosphorylated progerin C-terminal peptide (**Supplementary Fig. 1b**). Taken together, these results show that both prelamin A and progerin are alternatively prenylated in the presence of FTIs and provide an explanation for the low efficiency of the FTI-based treatment tested on progeroid mouse models.

We next used HGPS cells and *Zmpste24*$^{-/-}$ mice to evaluate therapeutic strategies for HGPS aimed at preventing cross-prenylation of prelamin A. We hypothesized that the farnesylation of aberrant lamin A variants may also be targeted by drugs acting on the synthetic pathway of farnesyl pyrophosphate, a cosubstrate of farnesyltransferase and a precursor of geranylgeranyl pyrophosphate, the substrate of geranylgeranyltransferase I. Because statins and aminobisphosphonates are among the approved drugs used to block this metabolic pathway[21], we tested their effects on normal and HGPS human fibroblasts. Mass spectrometry analysis revealed that this combined treatment with statins (pravastatin) and aminobisphosphonates

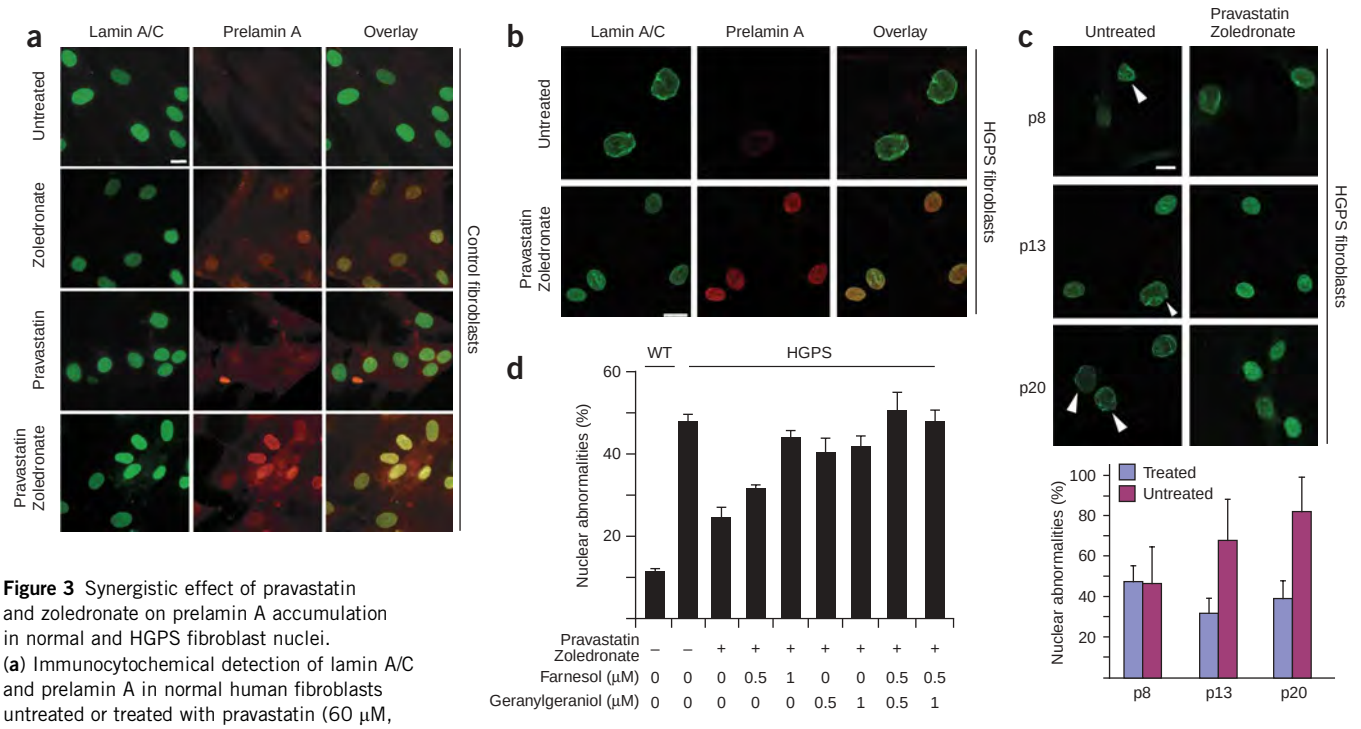

Figure 3 Synergistic effect of pravastatin and zoledronate on prelamin A accumulation in normal and HGPS fibroblast nuclei. (**a**) Immunocytochemical detection of lamin A/C and prelamin A in normal human fibroblasts untreated or treated with pravastatin (60 μM, 12 h) and zoledronate (60 μM, 6 h) alone or in combination. (**b**) Immunocytochemical detection of lamin A/C and prelamin A in normal and HGPS fibroblasts treated for 24 h with a combination of pravastatin (1 μM) and zoledronate (1 μM). (**c**) Quantification of the effects of the pravastatin (1 μM) and zoledronate (1 μM) combined treatment on nuclear morphology of HGPS cells. We analyzed untreated and treated cells with a lamin A/C-specific antibody at passages 8 (p8), 13 (p13) and 20 (p20). White arrowheads show representative images of misshapen nuclei. (**d**) Quantification of the effects of the pravastatin (1 μM) and zoledronate (1 μM) combined treatment on nuclear morphology of HGPS cells in the presence of either farnesol, geranylgeraniol or the combination of both. Error bars represent means ± s.e.m. Scale bars, 10 μm.

(zoledronate) causes the appearance of a peak corresponding to the molecular mass of the C-terminal nonprenylated peptide, which is undetectable in control or FTI-277–treated cells (**Supplementary Fig. 1c**). Of note, peaks corresponding to the farnesylated and geranylgeranylated peptides are absent in the spectra from pravastatin-zoledronate–treated HGPS cells, indicating that this treatment efficiently inhibits the prenylation of progerin (**Supplementary Fig. 1c**). We next investigated the effect of this combination of drugs on prelamin A maturation. The unprenylated C-terminal peptide is readily detectable in pravastatin-zoledronate–treated cells, whereas it is absent in control cells (**Supplementary Fig. 2** online). Conversely, the farnesylated and carboxyl-methylated peptide is present in control prelamin A but absent in the protein isolated from treated cells (**Supplementary Fig. 2**). Finally, in contrast to the effect of farnesyltransferase inhibition, the geranylgeranylated form is not detectable after pravastatin-zoledronate treatment (**Supplementary Fig. 2**).

To examine the potential benefits of this inhibition, we incubated HGPS cells with pravastatin, zoledronate or a combination of both compounds and analyzed nuclear morphology and prelamin A abundance. Immunocytochemical analysis of normal fibroblasts revealed an accumulation of prelamin A in the nuclear matrix of cells treated with the combination of pravastatin and zoledronate (**Fig. 3a**). HGPS-treated cells also accumulated prelamin A but, in addition, a clear improvement of their characteristic nuclear abnormalities was observed (**Fig. 3b**). Quantitative analysis of the effects of the combined pravastatin and zoledronate treatment on the nuclear morphology of HGPS cells revealed that the relative percentage of misshapen nuclei observed after successive passages decreased in HGPS-treated cells (**Fig. 3c**). To further investigate the effect of this treatment on the nuclear architecture of HGPS cells, we analyzed by immunofluorescence the distribution of lamin A/C and lamin B1 in control and treated cells (**Supplementary Fig. 3** online). Untreated HGPS cells contained nucleoplasmic aggregates of lamin A and lamin C isoforms, which can associate with deep invaginations of the inner nuclear envelope identifiable by calreticulin immunoreactivity (**Supplementary Fig. 3a–f**). These aggregates are absent from cells from healthy individuals (**Supplementary Fig. 3j–l**) and disappear upon pravastatin-zoledronate treatment (**Supplementary Fig. 3g–i**). The subcellular localization of lamin B1, a farnesylated nuclear lamina protein, underwent a similar change upon treatment with pravastatin-zoledronate (**Supplementary Fig. 3**), providing additional evidence of the potency of this combination of drugs to block isoprenylation of nuclear proteins.

To rule out the possibility that the observed decrease in the number of misshapen nuclei could be due to functions of pravastatin or zoledronate distinct from the blockade of progerin prenylation, we added farnesol or geranylgeraniol to the combined treatment of HGPS cells. Upon supplementation with farnesol or geranylgeraniol, cells should be able to generate farnesyl pyrophosphate or geranylgeranyl pyrophosphate, respectively, and then prenylate progerin even in the presence of pravastatin and zoledronate. We found that farnesol completely abolishes the effect of the pravastatin-zoledronate treatment on the nuclear morphology of HGPS cells (**Fig. 3d**), thus providing additional evidence that the efficacy of this treatment derives from its ability to inhibit farnesyl pyrophosphate synthesis. Notably, geranylgeraniol is also able to block this effect, showing that the geranylgeranylated form of progerin is toxic for progeria cells, as

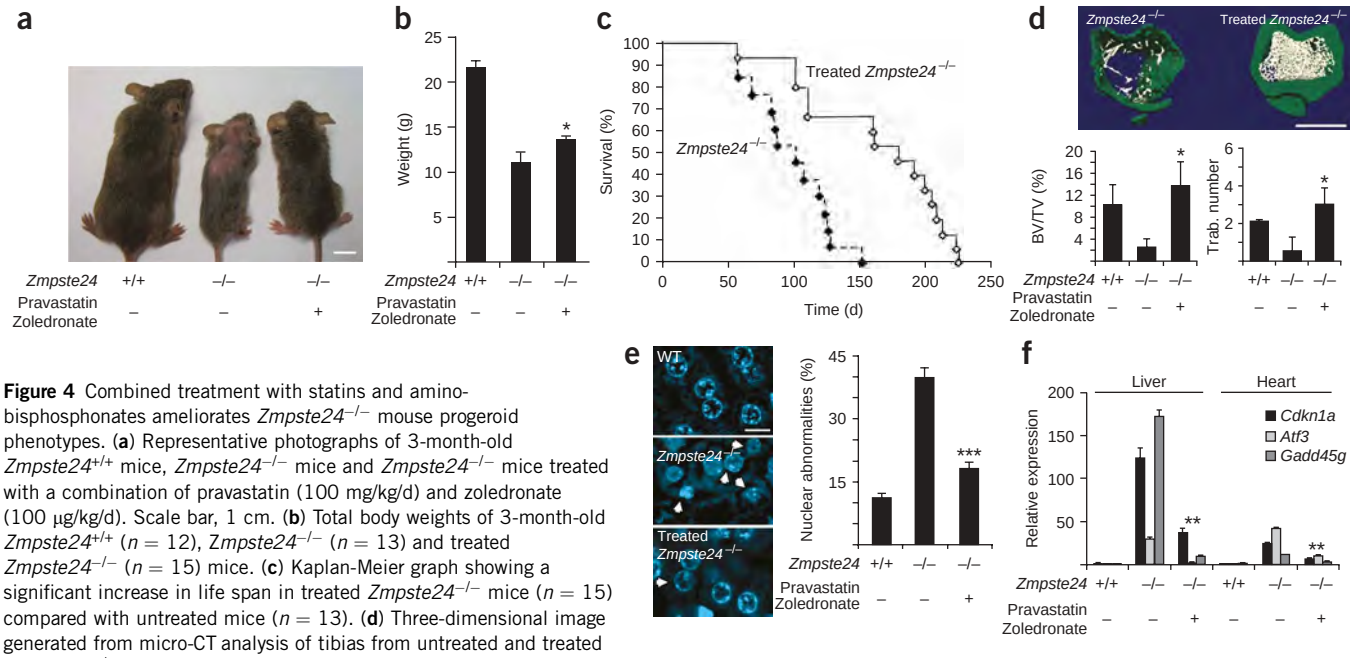

Figure 4 Combined treatment with statins and aminobisphosphonates ameliorates *Zmpste24*$^{-/-}$ mouse progeroid phenotypes. (**a**) Representative photographs of 3-month-old *Zmpste24*$^{+/+}$ mice, *Zmpste24*$^{-/-}$ mice and *Zmpste24*$^{-/-}$ mice treated with a combination of pravastatin (100 mg/kg/d) and zoledronate (100 μg/kg/d). Scale bar, 1 cm. (**b**) Total body weights of 3-month-old *Zmpste24*$^{+/+}$ ($n = 12$), *Zmpste24*$^{-/-}$ ($n = 13$) and treated *Zmpste24*$^{-/-}$ ($n = 15$) mice. (**c**) Kaplan-Meier graph showing a significant increase in life span in treated *Zmpste24*$^{-/-}$ mice ($n = 15$) compared with untreated mice ($n = 13$). (**d**) Three-dimensional image generated from micro-CT analysis of tibias from untreated and treated *Zmpste24*$^{-/-}$ mice (top). The bottom panel contains a representation of relative bone volume (bone volume / tissue volume, BV/TV) and number of trabecules/mm in wild-type *Zmpste24*$^{-/-}$ ($n = 6$) and treated *Zmpste24*$^{-/-}$ ($n = 5$) mice. Scale bar, 1 mm. (**e**) Quantification of nuclear abnormalities in livers from *Zmpste24*$^{+/+}$, *Zmpste24*$^{-/-}$ and treated *Zmpste24*$^{-/-}$ mice. White arrowheads show representative images of misshapen nuclei. Scale bar, 10 μm. (**f**) Relative expression of p53 targets in liver and heart from *Zmpte24*$^{+/+}$, *Zmpte24*$^{-/-}$ and treated *Zmpte24*$^{-/-}$ mice analyzed by quantitative RT-PCR. $^{*}P < 0.05$; $^{**}P < 0.01$; $^{***}P < 0.001$. Error bars represent means ± s.e.m.

well (**Fig. 3d**). These effects were also observed in *Zmpste24*$^{-/-}$ cells (**Supplementary Fig. 4a** online), indicating that the above findings for progerin can also be extended to prelamin A, which is the accumulated protein isoform in these *Zmpste24*$^{-/-}$ cells. Neither farnesol nor geranylgeraniol produced any effect on control fibroblasts, ruling out any potential artifact derived from the treatment with these compounds (**Supplementary Fig. 4b**). Finally, combined pravastatin-zoledronate treatment produced a reduction in phospho-H2AX foci accumulation, which correlates with DNA damage (**Supplementary Fig. 5** online). Taken together, these *in vitro* studies indicate that the combination of pravastatin and zoledronate partially blocks farnesylation and geranylgeranylation and leads to the expected nuclear lamina localization and nucleoplasmic redistribution of non-prenylated prelamin A in both normal and HGPS fibroblasts. Furthermore, we can conclude that both the reduced abundance of farnesylated progerin in the lamina and its relocalization in the nucleoplasm underlie the beneficial effect observed in HGPS cells after the continued combined treatment with pravastatin and zoledronate.

After these *in vitro* studies, we explored the effect of a treatment of statins and aminobisphosphonates on lifespan and progeroid phenotypes of *Zmpste24*$^{-/-}$ mice. Mutant mice and littermate controls were treated daily with zoledronate, pravastatin or a combination of both at doses previously used in mice with no evidence of toxicity[22,23]. Consistent with the above findings in HGPS-treated cells, we did not observe any survival benefit in *Zmpste24*$^{-/-}$ mice treated with either pravastatin or zoledronate alone (**Supplementary Fig. 6** online). In contrast, a substantial recovery of progeroid phenotypes was observed in *Zmpste24 Zmpste24*$^{-/-}$ mice with the combined treatment (**Fig. 4a–e**). Thus, the statin-aminobisphosphonate treatment improved body weight of *Zmpste24*$^{-/-}$ mice, increased the amount of subcutaneous fat, reduced the degree of kyphosis and alopecia and extended the longevity of mutant mice. The median survival of treated *Zmpste24*$^{-/-}$ mice was extended from 101 d to 179 d, and the maximum survival was extended from 151 d to 222 d ($P < 0.001$; **Fig. 4c**). Notably, all of the phenotypes rescued in *Zmpste24*$^{-/-}$ progeroid mice represent characteristic features of humans with HGPS. The combined treatment also resulted in a marked improvement of the bone density reduction that is a hallmark of both *Zmpste24*$^{-/-}$ mice and humans with HGPS or related progeroid syndromes[3,5]. Thus, microcomputerized tomography (micro-CT) analysis of *Zmpste24*$^{-/-}$ animals showed a marked increase in bone mineralization and cortical thickness when compared with untreated littermates (**Fig. 4d**). Additionally, quantification of nuclear abnormalities in livers from *Zmpste24*$^{+/+}$, *Zmpste24*$^{-/-}$ or treated *Zmpste24*$^{-/-}$ mice revealed that the pravastatin-zoledronate treatment induces a recovery of the shape of *Zmpste24*$^{-/-}$ nuclei to almost normal levels (**Fig. 4e**). Furthermore, we tested by quantitative RT-PCR the effect of this combined treatment on the upregulation of the p53 pathway described in *Zmpste24*$^{-/-}$ progeroid mice[8] and found a marked reduction in the abundance of all analyzed p53 targets in mutant mice (**Fig. 4f**). Finally, we evaluated whether this combined treatment could have any positive consequence on *Lmna*$^{-/-}$ mice, which present several phenotypes that resemble those observed in *Zmpste24*$^{-/-}$ mice but do not accumulate prenylated prelamin A[24]. However, the statin-aminobisphosphonate treatment failed to extend lifespan of *Lmna*$^{-/-}$ mice (**Supplementary Fig. 7** online), providing additional proof of the specificity of the treatment for mice that accumulate prenylated lamin A isoforms in the nuclear envelope.

The molecular mechanisms through which this combined treatment with statins and aminobisphosphonates ameliorates age-related phenotypes probably involve the blocking of prelamin A prenylation. Statins inhibit hydroxymethylglutaryl coenzyme A reductase, an enzyme located at the apex of the mevalonate pathway, whereas aminobisphosphonates act on the last steps of the same synthetic

pathway, inhibiting farnesyl pyrophosphate synthase and isopentenyl pyrophosphate isomerase[21]. The observed additive or synergistic effect of statins and bisphosphonates on *Zmpste24*$^{-/-}$ aging-like phenotypes may derive from their sequential action on different enzymes of the mevalonate pathway, thereby blocking both protein farnesylation and geranylgeranylation and minimizing the possibility of alternative prenylation events that confer resistance to FTIs. The above experiments showing that farnesol and geranylgeraniol abolish the positive effect of the pravastatin-zoledronate treatment on both HGPS and *Zmpste24*$^{-/-}$ cells support the proposal that these compounds exert their beneficial action through inhibition of prenylation of lamin A isoforms. Nevertheless, this combined pravastatin-zoledronate treatment may have additional effects derived from functions of statins and aminobisphosphonates distinct from their protein prenylation-blocking actions. Thus, statins—widely used as lipid-lowering drugs—also inhibit the synthesis of cholesterol, have extensive immunomodulatory properties and target the proteasome degradation machinery[25,26], whereas aminobisphosphonates have strong antiosteoporotic properties and block angiogenesis through mechanisms that may be independent from their inhibitory actions on the mevalonate pathway[22,27]. All of these pleiotropic effects of statins and aminobisphosphonates might contribute to an overall improvement in the health of *Zmpste24*$^{-/-}$ progeroid mice beyond the proposed action of these drugs in targeting the farnesylated forms of prelamin A that cause progeria. Nevertheless, many clinical studies have revealed that statins and aminobisphosphonates are well tolerated and are proven to be effective without showing any major negative effects after prolonged treatments. Furthermore, combinations of both compounds have been previously assayed in different *in vitro* and *in vivo* studies that have showed synergistic effects and no evidence of overlapping toxicities[28,29]. Accordingly, we propose that it should be worth exploring the combined potential of these drugs as a therapeutic approach to slow down disease progression in children with progeria.

METHODS

Mice. We generated and genotyped *Zmpste24*$^{-/-}$ and *Lmna*$^{-/-}$ mice as described[6,24]. We performed micro-CT analysis of bones with a micro-CT SkyScan 1172 system (SkyScan). We performed animal experimentation in accordance with the guidelines of the Committee for Animal Experimentation of the Universidad de Oviedo. We administrated pravastatin (100 mg/kg/d) and zoledronate (100 μg/kg/d) in PBS intraperitoneally to mice every day. Neither vehicle alone nor pravastatin-zoledronate treatments produced any apparent damage or stress responses in control mice.

Cell culture. We obtained human skin fibroblasts from a control subject (GM00038) and from subjects with HGPS carrying the G608G mutation (AG11498 and AG01972) from the Coriell Cell Repository. We obtained HeLa cells from the American Type Culture Collection. We maintained all cultures in DMEM (Gibco) supplemented with 10% FBS (Gibco) and 1% antibiotic-antimycotic (Gibco). We extracted mouse fibroblasts from 12-week-old mouse ears as previously described[8]. Doses and duration of treatments with statins and bisphosphonates are indicated in the figure legends. In combined treatment of statins and aminobisphosphonates with farnesol or geranylgeraniol, we added 1 μM of both pravastatin and zoledronate to culture medium together with increasing amounts of either farnesol, geranylgeraniol or both. We measured the percentage of misshapen nuclei 48 h after the start of treatment.

Immunocytochemistry. We transferred fibroblasts on Lab Tek chamber slides (Nalgen Nunc International), washed them with PBS and fixed them in 4% paraformaldehyde for 15 min. We dehydrated the fixed cells in ethanol and permeabilized them with 0.5% Triton X-100, 5% normal serum (goat or rabbit) in PBS for 5 min at 25 °C. Then we preincubated the slides at 25 °C in PBS supplemented with 5% normal serum. The primary antibody dilutions used were 1:100 for the prelamin A–specific goat polyclonal antibody (Sc-6214, Santa Cruz Biotechnologies), 1:40 for the mouse lamin A/C–specific antibody (4A7 kindly provided by G. Morris); 1:200 for the rabbit calreticulin-specific antibody (Stressgen), and 1:100 for the lamin B1–specific antibody (Abcam). After washes with PBS, we incubated the slides with secondary antibodies diluted in the incubation solution for 1 h at 25 °C. The secondary antibodies dilutions used were 1:100 FITC-conjugated mouse-specific donkey IgG (Jackson ImmunoResearch), 1:400 goat-specific Alexa 488–conjugated donkey IgG, 1:800 goat-specific Alexa 568–conjugated donkey IgG (Molecular Probes) and 1:100 rabbit-specific tetramethylrhodamine isothiocyanate–conjugated donkey IgG (Sigma). We then washed the cells and stained nuclei with DAPI (Sigma-Aldrich) at 100 ng/ml for 15 min at 25 °C and then washed three times in Tween-20 at 0.5% in PBS. Slides were mounted in Vectashield mounting medium (Vector). Digitalized microphotographs were recorded with a Leica DMR microscope equipped with a CoolSNAP camera or a Leica TCS SP5 laser confocal microscope. We counted normal and abnormal nuclei in chambers stained for lamin A/C. More than 100 nuclei of normal fibroblasts were counted for each treatment. The number of nuclei counted for HGPS fibroblasts was $n = 250$ at passage 8, $n = 198$ at passage 13 and $n = 150$ at passage 20.

X-ray irradiation and analysis of phosphorylated H2AX. We used a Philips X-ray clinical irradiator to irradiate HGPS cells and 1BR3 control fibroblasts. The X-ray beam was produced from a tungsten anode, applying a voltage setting of 200 kV and an intensity of 20 mA and using a filtration of 0.1 mm copper filter. The dose-rate was 1.234 Gy/min. We detected phosphorylated histone H2AX by immunofluorescence with antibodies specific for phosphorylated H2AX at Ser139 from Upstate Biotechnology-Euromedex (Mundolsheim, France), used at 1:800 dilution, followed by incubation with mouse-specific FITC-conjugated secondary antibodies (1:100; Sigma-Aldrich). We fitted the number of double-strand breaks as a function of repair time to the formula $N_t = N_0\ (1 / 1 + \beta t)^{\alpha}$, with α and β representing adjustable parameters and N_t and N_0 representing the number of double-strand breaks at time t and time 0.

Western blotting. We homogenized cells in 50 mM Tris (pH 7.4), 150 mM NaCl, 1% NP-40, 50 mM NaF, 1 mM dithiothreitol, 2 mg/ml pepstatin A, Complete inhibitor cocktail (Roche) and Phosphatase Inhibitor Cocktails I and II (Sigma). After electrophoresis, we transferred the protein extracts to nitrocellulose membranes, blocked with 5% nonfat dry milk in TBS-T buffer (20 mM Tris pH 7.4, 150 mM NaCl and 0.05% Tween-20) and incubated for 1 h with 3% nonfat dry milk in TBS-T with either 1:500 lamin A/C–specific (4A7), 1:250 lamin A–specific (C20, Santa Cruz Biotechnology) or 1:5,000 β-actin–specific (A5441, Sigma) antibodies. Finally, we incubated the blots with 1:10,000 of goat to mouse or rabbit to goat horseradish peroxidase (Jackson ImmunoResearch) in 1.5% nonfat milk in TBS-T, washed them and developed the immunoreactive bands with Immobilon Western chemiluminescent HRP substrate (Millipore).

Mass spectrometry analysis. We collected *Zmpste24*$^{-/-}$ and control mouse fibroblasts as well as HGPS lymphoblastoid cells, and, after homogeneization, we isolated nuclei by ultracentrifugation and used them to obtain nuclear lamina proteins as previously described[30]. We separated nuclear lamina proteins by SDS-PAGE and excised gel bands containing lamin, prelamin A or progerin. We washed gel pieces twice with 180 μl of 25 mM ammonium bicarbonate/acetonitrile (70:30), dried them for 15 min at 90 °C, and incubated them with 12 ng/μl trypsin (Promega) in 25 mM ammonium bicarbonate. We allowed the digestion to proceed for 1 h at 60 °C. In a typical experiment, 1 μl of CHCA (α-cyano-4-hydroxycinnamic acid, Waters) was placed onto a matrix-assisted laser desorption/ionization–time of flight (MALDI-ToF) plate. Once dried, we placed 1 μl of peptide mixture and 1 μl of matrix (CHCA) over it and performed mass spectrometry analysis on a time-of-flight mass spectrometer equipped with a nitrogen laser source (Voyager-DE STR, Applied Biosystems). We collected data from 200 laser shots to produce mass spectra and analyzed them with Data Explorer version 4.0.0.0 (Applied Biosystems).

Real-time quantitative PCR. We analyzed expression levels of selected p53 target genes (*Atf3*, *Gadd45g* and *Cdkn1a*, which encodes p21) with Applied Biosystems Taqman gene expression assays in an ABI PRISM

7900HT Sequence detection system (Applied Biosystems) following the manufacturer's instructions.

Statistical analysis. We performed statistical analysis of differences between mouse cohorts or treated and untreated cells with Student's *t*-test. We used Microsoft Excel for calculations and expressed the results as the mean ± s.e.m.

Note: Supplementary information is available on the Nature Medicine website.

ACKNOWLEDGMENTS

We thank G. Morris (Centre for Inherited Neuromuscular Disease, RJAH Orthopaedic Hospital) for antibody 4A7. We thank X.S. Puente, C.L. Ramírez, A.F. Braña, P. Bourgeois, C. Massart, F. Canals, M. Barbacid, C. Guerra, K. Tryggvason, C. Stewart and G. Velasco for helpful comments and advice and F. Rodríguez, S. Alvarez, E. Francezon, L. Espinosa and I. Bocaccio for excellent technical assistance. This work was supported by grants from Ministerio de Educación y Ciencia-Spain, Fundación La Caixa, Fundación M. Botín, Institut National de la Santé et de la Recherche Médicale-France, Agence Nationale de la Recherche-France, Association Française contre les Myopathies and the European Union (FP6 CancerDegradome and FP6 Eurolaminopathies). The Instituto Universitario de Oncología is supported by Obra Social Cajastur-Asturias.

AUTHOR CONTRIBUTIONS

I.V., A.P.U., J. Cadiñanos, F.G.O. and J.M.P.F. carried out animal experiments. S.P., C.L.N., P.C., N.F., I.V. and A.P.U. performed cell-culture based studies. I.V., J. Cadiñanos, J.M.P.F. and M.F.S. carried out mass spectrometry experiments. F.d.C. and J. Cobo conducted micro-CT analysis. C.L.-O., J.M.P.F., P.C. and N.L. were responsible for designing and supervising the project and writing the manuscript.

Published online at http://www.nature.com/naturemedicine/
Reprints and permissions information is available online at http://npg.nature.com/reprintsandpermissions/

1. Navarro, C.L., Cau, P. & Levy, N. Molecular bases of progeroid syndromes. *Hum. Mol. Genet.* **15** Suppl 2, R151–R161 (2006).
2. Scaffidi, P. & Misteli, T. Lamin A–dependent nuclear defects in human aging. *Science* **312**, 1059–1063 (2006).
3. Young, S.G., Meta, M., Yang, S.H. & Fong, L.G. Prelamin A farnesylation and progeroid syndromes. *J. Biol. Chem.* **281**, 39741–39745 (2006).
4. Kipling, D., Davis, T., Ostler, E.L. & Faragher, R.G. What can progeroid syndromes tell us about human aging? *Science* **305**, 1426–1431 (2004).
5. Hennekam, R.C. Hutchinson-Gilford progeria syndrome: review of the phenotype. *Am. J. Med. Genet. A.* **140**, 2603–2624 (2006).
6. Pendás, A.M. *et al.* Defective prelamin A processing and muscular and adipocyte alterations in Zmpste24 metalloproteinase–deficient mice. *Nat. Genet.* **31**, 94–99 (2002).
7. Ramirez, C.L., Cadinanos, J., Varela, I., Freije, J.M. & López-Otín, C. Human progeroid syndromes, aging and cancer: new genetic and epigenetic insights into old questions. *Cell. Mol. Life Sci.* **64**, 155–170 (2007).
8. Varela, I. *et al.* Accelerated ageing in mice deficient in Zmpste24 protease is linked to p53 signalling activation. *Nature* **437**, 564–568 (2005).
9. Liu, B. *et al.* Genomic instability in laminopathy-based premature aging. *Nat. Med.* **11**, 780–785 (2005).
10. Liu, Y., Rusinol, A., Sinensky, M., Wang, Y. & Zou, Y. DNA damage responses in progeroid syndromes arise from defective maturation of prelamin A. *J. Cell Sci.* **119**, 4644–4649 (2006).
11. Espada, J. *et al.* Nuclear envelope defects cause stem cell dysfunction in premature-aging mice. *J. Cell Biol.* **181**, 27–35 (2008).
12. Cadiñanos, J., Varela, I., López-Otín, C. & Freije, J.M. From immature lamin to premature aging: molecular pathways and therapeutic opportunities. *Cell Cycle* **4**, 1732–1735 (2005).
13. Toth, J.I. *et al.* Blocking protein farnesyltransferase improves nuclear shape in fibroblasts from humans with progeroid syndromes. *Proc. Natl. Acad. Sci. USA* **102**, 12873–12878 (2005).
14. Capell, B.C. *et al.* Inhibiting farnesylation of progerin prevents the characteristic nuclear blebbing of Hutchinson-Gilford progeria syndrome. *Proc. Natl. Acad. Sci. USA* **102**, 12879–12884 (2005).
15. Mallampalli, M.P., Huyer, G., Bendale, P., Gelb, M.H. & Michaelis, S. Inhibiting farnesylation reverses the nuclear morphology defect in a HeLa cell model for Hutchinson-Gilford progeria syndrome. *Proc. Natl. Acad. Sci. USA* **102**, 14416–14421 (2005).
16. Glynn, M.W. & Glover, T.W. Incomplete processing of mutant lamin A in Hutchinson-Gilford progeria leads to nuclear abnormalities, which are reversed by farnesyltransferase inhibition. *Hum. Mol. Genet.* **14**, 2959–2969 (2005).
17. Fong, L.G. *et al.* A protein farnesyltransferase inhibitor ameliorates disease in a mouse model of progeria. *Science* **311**, 1621–1623 (2006).
18. Yang, S.H. *et al.* A farnesyltransferase inhibitor improves disease phenotypes in mice with a Hutchinson-Gilford progeria syndrome mutation. *J. Clin. Invest.* **116**, 2115–2121 (2006).
19. Whyte, D.B. *et al.* K- and N-Ras are geranylgeranylated in cells treated with farnesyl protein transferase inhibitors. *J. Biol. Chem.* **272**, 14459–14464 (1997).
20. Rusinol, A.E. & Sinensky, M.S. Farnesylated lamins, progeroid syndromes and farnesyl transferase inhibitors. *J. Cell Sci.* **119**, 3265–3272 (2006).
21. Konstantinopoulos, P.A. & Papavassiliou, A.G. Multilevel modulation of the mevalonate and protein-prenylation circuitries as a novel strategy for anticancer therapy. *Trends Pharmacol. Sci.* **28**, 6–13 (2007).
22. Giraudo, E., Inoue, M. & Hanahan, D. An amino-bisphosphonate targets MMP-9–expressing macrophages and angiogenesis to impair cervical carcinogenesis. *J. Clin. Invest.* **114**, 623–633 (2004).
23. Yamagata, T. *et al.* Effects of pravastatin in murine collagen-induced arthritis. *Rheumatol. Int.* **27**, 631–639 (2007).
24. Sullivan, T. *et al.* Loss of A-type lamin expression compromises nuclear envelope integrity leading to muscular dystrophy. *J. Cell Biol.* **147**, 913–920 (1999).
25. Demierre, M.F., Higgins, P.D., Gruber, S.B., Hawk, E. & Lippman, S.M. Statins and cancer prevention. *Nat. Rev. Cancer* **5**, 930–942 (2005).
26. Greenwood, J., Steinman, L. & Zamvil, S.S. Statin therapy and autoimmune disease: from protein prenylation to immunomodulation. *Nat. Rev. Immunol.* **6**, 358–370 (2006).
27. Roelofs, A.J., Thompson, K., Gordon, S. & Rogers, M.J. Molecular mechanisms of action of bisphosphonates: current status. *Clin. Cancer Res.* **12**, 6222s–6230s (2006).
28. Issat, T. *et al.* Potentiated antitumor effects of the combination treatment with statins and pamidronate in vitro and in vivo. *Int. J. Oncol.* **30**, 1413–1425 (2007).
29. Schmidmaier, R., Simsek, M., Baumann, P., Emmerich, B. & Meinhardt, G. Synergistic antimyeloma effects of zoledronate and simvastatin. *Anticancer Drugs* **17**, 621–629 (2006).
30. Blobel, G. & Potter, V.R. Nuclei from rat liver: isolation method that combines purity with high yield. *Science* **154**, 1662–1665 (1966).